Modelling water-rock interactions due to long-term cooled-brine reinjection in the Dogger carbonate aquifer (Paris basin) based on in-situ geothermal well data

Nicolas C.M. Marty, Virginie Hamm, Christelle Castillo, Dominique Thiéry, Christophe Kervévan

Modelling water-rock interactions due to long-term cooled-brine reinjection in the Dogger carbonate aquifer (Paris basin) based on in-situ geothermal well data

Nicolas C.M. Marty[a*], Virginie Hamm[a], Christelle Castillo[a], Dominique Thiéry[a], Christophe Kervévan[a]

[a] BRGM, 3 Avenue Claude Guillemin, Orléans Cedex 2, 45064, France

* Corresponding author

Email: n.marty@brgm.fr

Address: BRGM, D3E/SVP, 3 Avenue Claude Guillemin, F-45060 Orléans, Cedex 2, France

Tel.: +33 2 38 64 33 43

Abstract

An experimental campaign was conducted using bottom-hole geometry data from a 24-year-old injection well (~1700 m deep) at a geothermal site exploiting the Dogger aquifer (Paris basin). A sonar tool was used to measure the geometry distortion of the open hole due to long-term reinjection of cooled brine. Reactive transport modelling was then performed. The calculated extent of carbonate dissolution at the well outlet was consistent with the sonar observations. The best fit to experimental results was obtained by considering partial CO_2 degassing in the reinjected brine, which is consistent with the artesian mode doublet operation.

Keywords: geothermal doublet, porosity, Dogger aquifer, water-rock interaction, geochemical modelling, sonar

1. Introduction

Located at a depth of 1500–2000 m, the carbonate Dogger reservoir is the main geothermal aquifer exploited in the Paris region of France. This geothermal resource heats approximately 210,000 dwellings in the Ile-de-France region [1] through a significant growth objective defined by the French energy transition law (http://www.gouvernement.fr/en/energy-transition). Energy exploitation involves the reinjection of cooled brine into the carbonated reservoir after calorie extraction by heat exchangers [e.g. 1, 2, 3]. The local reinjected fluid temperature depends on the production temperature (55–85 °C), the energy requirements at the surface, and the operating flowrate (100–350 m^3 h^{-1}) and typically varies between 40 and 60 °C with a minimum temperature of 35 °C. All geothermal operations from the 1970s to 1990s operated according to this principle [2]; however, more recent geothermal operations conducted in the Dogger aquifer employ a heat pump (e.g. Arcueil-Gentilly, Bagneux, Neuilly-sur-Marne, etc.) to optimise the available geothermal resource, resulting in a lower return temperature. This implies that reinjection of cooled brines at the Dogger aquifer occurs at lower temperatures (approximately 25 °C) than previously [4].

To date, the majority of studies on the thermal effect on Dogger formation geochemistry have focused on the hydro-geochemical impact of the reinjection of hot fluids into the aquifer from the perspective of heat storage [5, 6]. Only a few studies have quantified the hydro-geochemical impact of cooled-fluid reinjection in a carbonate aquifer [7-9]. Geothermal energy production in the carbonate Dogger formation began in the early 1970s in the Paris basin [2]. The typical lifetime of a geothermal doublet is approximately 30 years (duration of the initial operating permits); therefore, as older wells are shut down, new wells are commissioned. Thus, bottom-hole analysis of former injection wells could allow us to observe and quantify the effects of potential water-rock interactions induced by cooled-brine reinjection, especially in a carbonate aquifer such as the Dogger. Unfortunately, most of these wells were plugged when the abandonment procedure was completed and are thus inaccessible. However, as part of the CO_2-DISSOLVED project and through collaboration with the local geothermal operator (Chelles Chaleur, subsidiary of the Coriance group), the unique opportunity was granted to access the open-hole part of a former injection well in Chelles (Paris basin, France). This injector was utilised for 24 years from 1986 to 2010 but remains accessible as a backup injection well for the current geothermal doublet. An in-situ experimental campaign was conducted in March 2016 to analyse the reservoir geometry at the well outlet using an innovative sonar tool provided and operated by Flodim (Cavity Survey and Well Logging Services Company, https://www.flodim.fr/).

The results of this study will aid our understanding of water-rock interactions at the well outlet, which is a major concern of the CO_2-DISSOLVED project (http://co2-dissolved.brgm.fr/). CO_2-DISSOLVED is an innovative carbon capture and storage (CCS) concept involving the capture, injection, and storage of dissolved CO_2 (rather than supercritical) in a deep saline aquifer coupled with geothermal heat recovery [10-12]. Once out of the injection well, the acidified brine is expected to be chemically reactive with the reservoir porous matrix, particularly in the presence of carbonate minerals [13-15]. In order to quantify these effects, both experimental and numerical modelling studies have been conducted in parallel as part of the CO_2-DISSOLVED project. The most notable results were obtained with the carbonate samples, showing the rapid development of a network of wormholes around the injection pipe outlet [16]. A numerical simulation of this experiment performed with the MARTHE-PHREEQC code [17] reproduced the massive dissolution of calcite near the injection pipe and the formation of wormholes due to the heterogeneous hydraulic conductivity reasonably accurately [18]. As demonstrated in numerous studies, the formation of wormholes depends on several parameters such as the ratios of reaction rate, convection rate and diffusion rate (i.e. Peclet and Damköhler numbers) [15, 18, 19] and material heterogeneities (i.e. permeability and chemical composition) [18, 20]. Regarding the Chelles doublet, no dissolved CO_2 has been added in the injected cooled brine. Contrariwise, the artesian production mode of the doublet led to CO_2 degassing at surface. Near neutral pH of the reinjected brine resulted in a solution close to equilibrium with respect to calcite and therefore, the Damköhler number was low, thus promoting uniform dissolution [15, 18].

The aim of this study is to provide reference data for the predicted effects of reactive processes at the well outlet when reinjecting a cooled brine (i.e. a ‘standard’ cooled geothermal brine). Moreover, it is critical to be able to compare the modelling results to actual bottom-hole measured data in order to evaluate the validity of model predictions. In contrast to other geothermal reservoirs [e.g. 21, 22], such reservoir data are extremely scarce for the Dogger carbonate aquifer and have not previously been made available to the scientific community; therefore, this study provides insights into water-rock interactions in this specific environment. The second objective of this study is to give insights to better interpret predictions of the CO_2-DISSOLVED system related to adding dissolved CO_2 to the reinjected brine. This is because this CCS method has not yet been tested at full scale, so no equivalent in-situ data can be obtained; therefore, modelling remains the only approach to estimate the potential impacts of dissolved CO_2 reinjection on the exploited reservoir. In a such context, the hole stability [23] and permeability increase leading to a risk of thermal breakthrough in the nearby production wells [13, 24] are intensively investigated.

2. Materials and methods

2.1. Chelles geothermal doublet

The Chelles geothermal district heating doublet was exploited continuously since its commissioning in 1986 until its closure in 2010 in artesian production mode with a maximal flow rate of 250 m^3 h^{-1} (Figure 1). This system operated at high flow rates and a wellhead pressure lower than the bubble point, leading to the partial release of gases initially dissolved in the Dogger pore water and their partial trapping high in the geothermal pipe [25]. The geothermal reservoir has a gas production capacity of approximately 0.125 m^3 per m^3 of Dogger fluid. The gas phase is mainly composed of CH_4 and other alkanes (55%), N_2 (35%), and CO_2 (10%) [25-27]. From 2000–2010, a special degassing device was employed for gas extraction and burning [25]. Unfortunately, gas extraction was not monitored over time; therefore, the partial pressure of CO_2 in equilibrium with the reinjected fluids remains uncertain. In contrast, flow and temperature data of the Chelles doublet GCHE1/GCHE2 are available from the Dogger database (https://dogger-idf.brgm.fr); however, data regarding the injection well are very sporadic between 1986 and 2010 (see injection_history file in Electronic Annex). Indeed, only typical injections have been recorded during winters of the first 5 years (one recording per year) and data are not continuous between years 5 to 24 years (about one recording per month). Therefore, average flow rates and injection temperatures of the injection well (GCHE1) during summer (133 m^3 h^{-1} and 52 °C) and winter (148 m^3 h^{-1} and 48 °C) were considered in this study. Such a discretisation in two steps is supported by recorded data from similar doublets in the Paris basin [2]. Conversely, a constant temperature of 66 °C was monitored at the production well (GCHE2).

The section of the GCHE1 well has been drilled in 1985 with a diameter of 8½" (Figure S1). However, the exact geometry of the injection chamber has not been determined after the drilling operation (i.e. no caliper measurement). Nonetheless, the numerous drilling operations carried out in the Dogger aquifer do not indicate any enlargement/damage of the borehole. In particular, the GCHE4 well that has been drilled in 2013 at the immediate vicinity of GCHE1, using similar operational conditions in terms of tool (rotary drilling), geometry (8½" diameter), and geological formation targeted (Dogger aquifer). Caliper data are available for GCHE4 and they confirm an effective diameter of the open hole consistent with the nominal drilling diameter. As a consequence, we assumed an initial radius of 0.1 m for the open hole of the GCHE1 injection well. Regarding the structure of the geothermal reservoir, the GCHE1 well is characterised by five productive layers of the Dogger aquifer [2, 28]: two layers of Comblachian units from -1668 m to -1683 m FOD (French Ordnance Datum), which contribute up to 14.7% of the total flow, and three layers of Oolithic units from

-1692 m to -1709 m FOD, contributing 85.3% of the total flow. The porosity, permeability, and flow contribution of each layer are summarised in Table 1. Measured permeabilities are greater than the one of the Oolithic limestone studied by Randi et al. [18] (i.e. 88 mD). Such values may reflect the presence of fractures in the Dogger aquifer. This also raises the question about the representativeness of the sample studied by the authors.

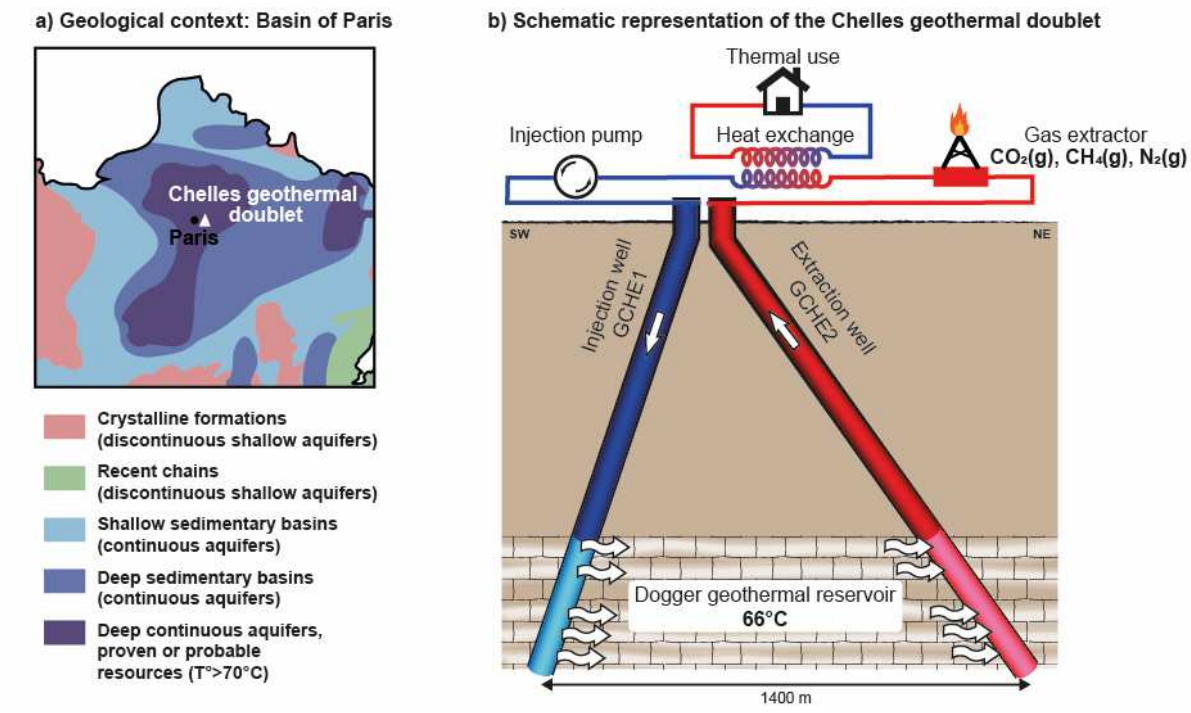

Figure 1. Location and schematic representation of the Chelles geothermal doublet.

Table 1. Production levels identified by flowmetry analyses conducted in 1985.

Facies	Layer	Altitude (m FOD*)	Flow contribution (%)	Porosity (%)	Permeability (D)
Comblachian	1	-1667.8 / -1669.8	7.3	12.5	1.03
	2	-1682.4 / -1683.3	7.4	15.8	2.09
Oolithic	3	-1692.1 / -1698.4	29.4	17.4	1.28
	4	-1702.3 / -1703.7	51.0	15.7	9.60
	5	-1707.1 / -1708.6	4.9	14.9	0.92

**French Ordnance Datum*

2.2. Examination of the injection well post-geothermal production

149 The injection well (GCHE1) integrity was examined in March 2016 by combining ABI
150 technique (Acoustic Borehole Imaging) and a sonar tool developed by Flodim. The technical
151 principle of the sonar probe involves sound propagation (at lower frequency than for ABI) and
152 recording the reflection of the acoustic signal against the cavity wall. The cavity wall is clearly
153 imaged if the density contrast between the fluid and the ground is strong and the wall is
154 regular. The measurement range is several centimetres to hundreds of metres. Currently,
155 sonar does not allow continuous acquisition. The probe performs 360° rotations with a fixed
156 measurement step (5° in this study) at a fixed depth. Once the rotation is complete, the probe
157 moves to another depth to resume measurements.

158

159 ***2.3. Numerical tools***

160 MARTHE-PHREEQC reactive transport modelling software is an extension of MARTHE
161 software [http://marthe.brgm.fr/, 17], which has been upgraded by coupling with the
162 PHREEQC chemical module [29]. The coupling algorithm is purely sequential; at each time
163 step, MARTHE computes the hydraulic head field and hence the velocity in the entire
164 domain. It then transports all considered dissolved chemical elements and also transports
165 heat to determine the temperature field on which geochemical reactions depend. Then, the
166 geochemistry is computed using the PHREEQC module. The THERMODDEM
167 thermodynamic database [30] (http://thermoddem.brgm.fr/) was used in this study. The B-dot
168 model, an extension of the Debye-Hückel activity model, is valid up to salinities of about 1
169 mol L^{-1} [31, 32].

170 **3. Experimental results**

171 The cavity extension was measured by the sonar tool at depths of approximately every 0.5
172 m. Investigations were focused on the exploited part of the geothermal reservoir (from -1650
173 to -1710 m FOD), where the well is characterised by the absence of open-hole casing.
174 Maximum and minimum extensions are reported in Figure 2. The shape and volume of the
175 cavity were irregular in both horizontal and vertical orientations. Nonetheless, regardless of
176 the amount of dissolved rock, preferential alteration leading to cavity formation was clearly
177 identified in the SW direction. This observation fully agrees with the tilt of the GCHE1 well
178 (Figure 1); i.e., the direction of injected flow strongly influences the shape of the formed
179 cavity. Note that ABI data (GCHE1_ABI file in Electronic Annex) of the well section located
180 below the productive layers do not indicate any enlargement/damage of the bore hole due to
181 drilling operations, thus supporting an initial open hole diameter of 0.1 m.

Surfaces and thus volumes of irregular polygons have been directly calculated by the tool software knowing the coordinates of the vertices and the thickness of the investigated area (Figure 3a). Despite the observed slight shift of data with depth, the productive layers identified in 1985 (Table 1) were in reasonable agreement with the maximum altered volumes of rock. These volumes were converted to equivalent radii, assuming a cylindrical geometry for the cavity (Figure 3b) following:

$$r_{eq} = \sqrt{\frac{V}{h \cdot \pi}} \qquad \text{(Eq. 1)}$$

where r_{eq} is the equivalent radius (m), V the volume given by the sonar tool (m^3) and h the thickness of the area investigated (m).

The average calculated radius was 0.21 m. Considering an initial well radius of 0.1 m, approximately 6 m^3 of the Dogger formation was dissolved during the operating period of the injection well (1986–2010). The average radius was compared with numerical results in order to evaluate the effect of various modelling assumptions (i.e. the geometry considered and the chemistry of the injection solution).

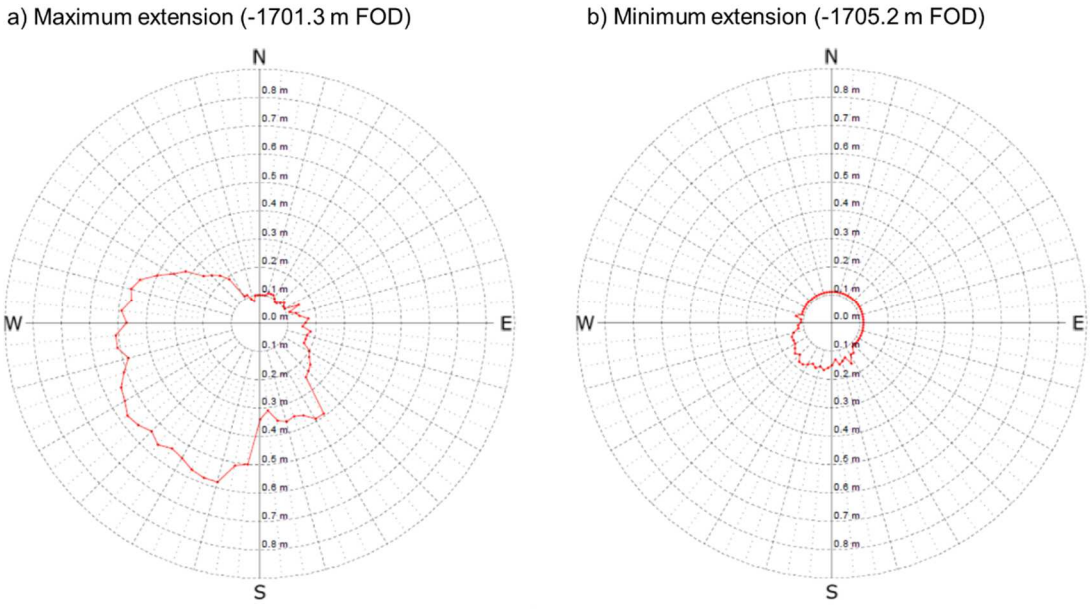

Figure 2. a) Maximum extension of the cavity observed at -1701.3 m FOD and b) minimum extension of the cavity observed at -1705.2 m FOD. Experimental data were measured by the sonar tool every ~0.5 m.

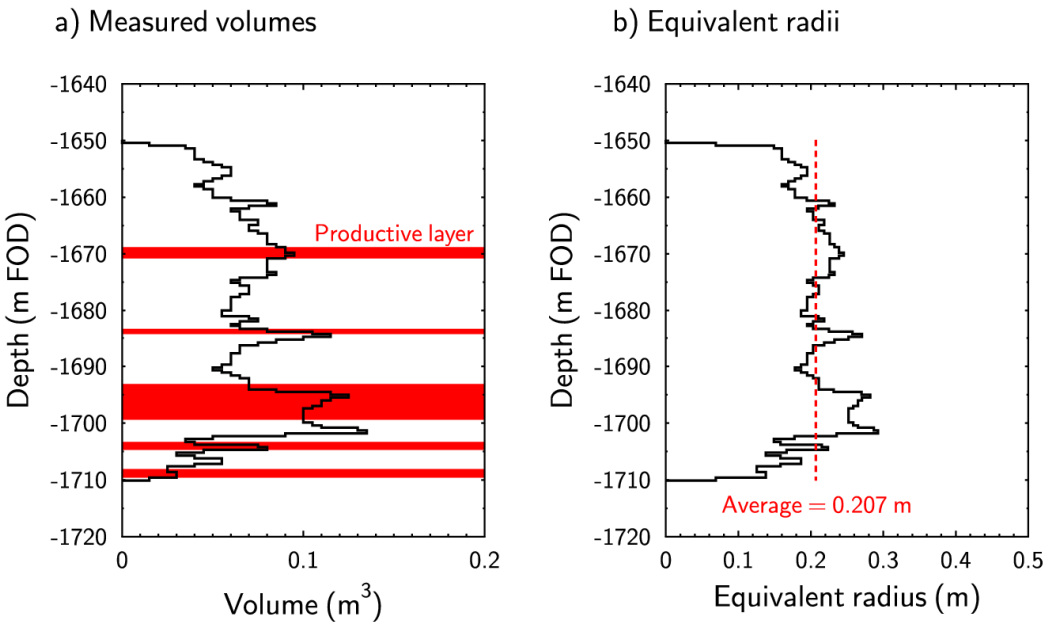

Figure 3. a) Volumes measured by the sonar tool every 0.5 m and b) calculated equivalent radii assuming a cylindrical cavity.

4. Modelling strategy

4.1. Dogger formation parameters

The mineralogical composition of the Dogger formation (Table 2) was established from the volume percentages given in [33] and [6]. The Dogger assemblage consists essentially of calcite and dolomite. Siderite, illite, albite, and K-feldspars are present as accessory minerals. The chemical composition of the Dogger brine was calculated for a temperature of 66 °C according to the value recorded at the production well. The simulation assumed a thermodynamic equilibrium between the Dogger pore water [13, 34] and the mineralogical assemblage reported in Table 2. Note that the formation of albite and K-feldspars is unlikely at 66 °C and only dissolution reactions occurred during equilibration. In addition, a CO_2 partial pressure of 100 mbar (log pCO_2 = -1.0 atm) was assumed for the Dogger formation. Such a partial pressure is in the lower range of values reported for this aquifer [35]. Constraints assumed for the fluid composition calculation are reported in Table 3. The fluid is in equilibrium with carbonates (calcite, dolomite, and siderite), illite, and quartz (Table 4). It is also close to equilibrium with sulphate bearing minerals such as barite ($BaSO_4$) and celestine ($SrSO_4$).

222 *Table 2. Mineralogical assemblage of the Dogger formation (data extracted from André, Audigane,*
223 *Azaroual and Menjoz [33] and Gille [6]).*

Mineral	Mineral name in THERMODDEM	Volume fraction
Calcite	Calcite	0.7
Dolomite-des	Dolomite(disordered)	0.1
Siderite	Siderite	0.05
Illite	Illite(IMt2)	0.05
Albite	Albite(low)	0.05
K-Feldspaths	Microcline	0.05

224

225 *Table 3. Chemistry of the Dogger pore water at 66 °C.*

Element	Concentration (mol L^{-1})	Constraint
Al	$1.67\ 10^{-07}$	Gibbsite
Ba	$1.09\ 10^{-06}$	Barite
C(4)	$5.24\ 10^{-03}$	P_{CO2}
Ca	$1.12\ 10^{-02}$	Calcite
Cl	$3.14\ 10^{-01}$	
Fe	$8.39\ 10^{-05}$	Siderite
K	$9.38\ 10^{-03}$	Illite(IMt2)
Mg	$1.63\ 10^{-02}$	Dolomite-des
Na	$2.70\ 10^{-01}$	
S(6)	$9.01\ 10^{-03}$	
Si	$5.06\ 10^{-04}$	Quartz
Sr	$5.23\ 10^{-04}$	
pH	6.48	
pe	-3.51	
log P_{CO2} (atm)	-1.0	

226

227 *Table 4. Saturation indices of the Dogger pore water at 66 °C (SI = log IAP/K, where IAP is the ionic*
228 *activity product and K the thermodynamic constant).*

Phases	Saturation indices (SI)
Calcite	0
Dolomite(disordered)	0
Siderite	0
Gibbsite	0
Illite(IMt2)	0
Albite(low)	0.48
Microcline	1.09
Quartz(alpha)	0
Celestite	-0.19
Barite	0

229

230 ***4.2. Chemistry of injected fluids***

231 The numerical simulations considered fluid reinjection at different temperatures according to
232 different periods (heat extraction being more important in cold periods). In the heat exchanger,
233 calculations did not consider the mineralogical assemblage of the Dogger because no mineral
234 phase was theoretically present. However, potential secondary phases such as calcite, and
235 barite were implemented. If oversaturated, their precipitation should occur primarily in the heat
236 exchanger and in the downstream pipe portion (i.e. in the coldest zone).

237 As a first approximation, CO_2 degassing was not considered and the fluid chemistry at 48 °C
238 and 52 °C was calculated from simple cooling of the Dogger pore water ("No degassing" case,
239 Table 5). As expected, the temperature decrease destabilises the carbonate minerals, which
240 are then undersaturated (Table 6). However, between 1986 and 2010, the Chelles geothermal
241 doublet operated in artesian mode, resulting in degassing at the wellhead that favoured
242 carbonate precipitation instead. A second model ("Partial degassing" case, Table 5) was then
243 established assuming partial degassing of CO_2 until a calcite saturation index of -0.01 (i.e.
244 almost in equilibrium with this carbonate). This value was adjusted to reasonably match with
245 the observed calcite dissolution using a single-layer geometry. Finally, a third solution
246 chemistry was calculated considering the CO_2 atmospheric partial pressure (i.e. $\log P_{CO2} = -3.45$
247 (atm)) related to calcite precipitation ("Total degassing" case, Table 5). Regardless of the fluid
248 chemistry (i.e. CO_2 degassing), the cooling of brines leads to barite and quartz precipitation
249 (Table 6). Nonetheless, silica precipitation is known to be a slow process at considered
250 temperatures [e.g. 37] and Si concentrations reported in Table 5 are probably under estimated.
251 Note that numerous studies have reported quartz, barite, and calcite scaling in geothermal wells

[e.g. 38, 39, 40]; however, this study was not focused on such surface and subsurface processes.

Table 5. Injected brine compositions as a function of temperature and CO_2 partial pressure.

Element	Concentrations (mol L^{-1})					
	No degassing		Partial degassing		Total degassing	
	48 °C	52 °C	48 °C	52 °C	48 °C	52 °C
Al	$4.15\ 10^{-08}$	$5.67\ 10^{-08}$	$6.02\ 10^{-08}$	$7.59\ 10^{-08}$	$1.67\ 10^{-07}$	$1.67\ 10^{-07}$
Ba	$7.12\ 10^{-07}$	$7.89\ 10^{-07}$	$7.12\ 10^{-07}$	$7.90\ 10^{-07}$	$6.94\ 10^{-07}$	$7.68\ 10^{-07}$
C(4)	$5.24\ 10^{-03}$	$5.24\ 10^{-03}$	$4.71\ 10^{-03}$	$4.80\ 10^{-03}$	$4.01\ 10^{-04}$	$3.70\ 10^{-04}$
Ca	$1.12\ 10^{-02}$	$1.12\ 10^{-02}$	$1.12\ 10^{-02}$	$1.12\ 10^{-02}$	$9.64\ 10^{-03}$	$9.63\ 10^{-03}$
Cl	$3.14\ 10^{-01}$	$3.14\ 10^{-01}$	$3.14\ 10^{-01}$	$3.14\ 10^{-01}$	$3.14\ 10^{-01}$	$3.14\ 10^{-01}$
Fe	$8.39\ 10^{-05}$	$8.39\ 10^{-04}$	$8.39\ 10^{-05}$	$8.39\ 10^{-05}$	$1.61\ 10^{-06}$	$1.25\ 10^{-06}$
K	$9.38\ 10^{-03}$	$9.38\ 10^{-03}$	$9.38\ 10^{-03}$	$9.38\ 10^{-03}$	$9.38\ 10^{-03}$	$9.38\ 10^{-03}$
Mg	$1.63\ 10^{-02}$	$1.63\ 10^{-02}$	$1.63\ 10^{-02}$	$1.63\ 10^{-02}$	$1.63\ 10^{-02}$	$1.63\ 10^{-02}$
Na	$2.70\ 10^{-01}$	$2.70\ 10^{-01}$	$2.70\ 10^{-01}$	$2.70\ 10^{-01}$	$2.70\ 10^{-01}$	$2.70\ 10^{-01}$
S(6)	$9.01\ 10^{-03}$	$9.01\ 10^{-03}$	$9.01\ 10^{-03}$	$9.01\ 10^{-03}$	$9.01\ 10^{-03}$	$9.01\ 10^{-03}$
Si	$3.30\ 10^{-04}$	$3.64\ 10^{-04}$	$3.30\ 10^{-04}$	$3.65\ 10^{-04}$	$3.40\ 10^{-04}$	$3.76\ 10^{-04}$
Sr	$5.23\ 10^{-04}$	$5.23\ 10^{-04}$	$5.23\ 10^{-04}$	$5.23\ 10^{-04}$	$5.23\ 10^{-04}$	$5.23\ 10^{-04}$
pH	6.50	6.49	6.70	6.64	7.78	7.77
pe	-3.24	-3.31	-3.50	-3.49	-4.77	-4.82
log P_{CO2} (atm)	-1.14	-1.11	-1.34	-1.26	-3.45	-3.45

Table 6. Saturation indices of injected brines as a function of temperature and CO_2 degassing (SI = log IAP/K, where IAP is the ionic activity product and K the thermodynamic constant).

Phases	Saturation indices (SI)					
	No degassing		Partial degassing		Total degassing	
	48 °C	52 °C	48 °C	52 °C	48 °C	52 °C
Calcite	-0.20	-0.16	-0.01	-0.01	0	0
Dolomite (disordered)	-0.59	-0.46	-0.21	-0.16	-0.12	-0.08
Siderite	-0.21	-0.17	-0.03	-0.03	-1.69	-1.79
Illite (IMt2)	-0.77	-0.59	-0.38	-0.30	-0.07	-0.23
Albite (low)	0.11	0.19	0.30	0.34	0.81	0.74
Microcline	0.96	0.99	1.16	1.14	1.66	1.54
Quartz (alpha)	0	0	0	0	0	0
Celestite	-0.24	-0.23	-0.24	-0.23	-0.23	-0.21
Barite	0	0	0	0	0	0
Goethite	-0.59	-0.48	-0.25	-0.22	0	0

4.3. Geometries and key modelling assumptions

Two distinct but simplified geometries were considered: homogeneous and heterogeneous (Figure 4). A single-layer homogeneous model was first applied to simulate the geothermal reservoir. The mesh was radial type with X, Y, and Z coordinates coinciding with the radius, angle, and layer of the model, respectively. A homogeneous porosity of 15% was assumed in the geological formation [i.e. average porosity, 2]. The model assumed upper and lower impervious walls following the approximate analytical solution of Vinsome and Westerveld [41] (thermal conduction perpendicular to the aquifer) implemented in MARTHE. This analytical solution avoiding the vertical discretization of the clay layers so considerably reduced the number of meshes in the model, thereby decreased the computation time. Note that a single-layer geometry leads to an over estimation of the cooling down of the reservoir [42], however, such an assumption is widely used when the knowledge of the geothermal reservoir is low (e.g. in the case of predictive modelling). Moreover, even if several productive layers have been identified (Table 1), the open hole extension shown on Figure 3b appears to be relatively homogeneous and thus a single layer geometry could be a correct assumption for assessing mineralogical transformations. A second, heterogeneous model was proposed using the Chelles injection well data (e.g. the productive layers identified by flowmeter, Table 1). The Dogger reservoir was discretised into five layers with specific properties. The mesh was also radial type and assumed upper and lower impervious walls using an analytic solution for the heat diffusion. Injected flows were distributed according to the contribution of the productive layers (Table 1). In contrast, according to flowmeter data, unproductive layers were considered as impervious layers only contributing to heat diffusion. The general parameters used for the simulations were defined using data from previous literature and are summarised in Table 7. A radial extension of 1000 m was assumed whatever the geometry considered.

a) Single-layer geometry

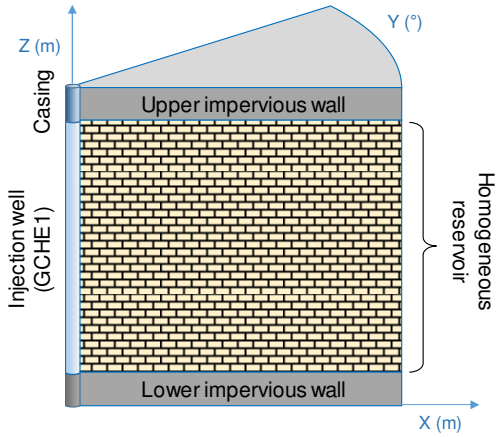

b) Multi-layer geometry

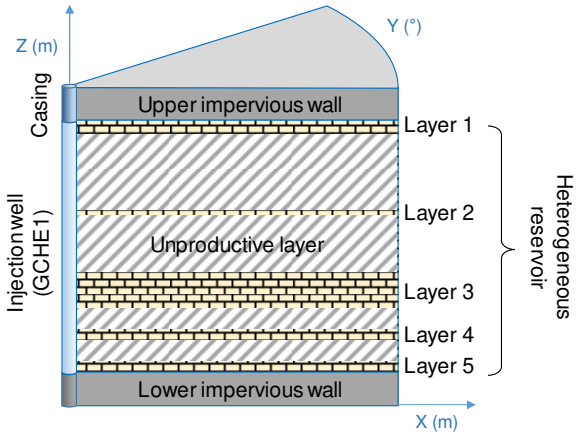

Figure 4. Schematic representations of the two model geometries: a) single-layer geometry and b) multi-layer geometry using flowmeter data from 1985.

Table 7. General parameters used for the simulations.

Simulation parameters	**Values**
Initial temperature (°C)	66
Volumetric heat capacity of the mineral (J m^{-3} $°C^{-1}$)	2 10^6
Heat capacity of the water (J kg^{-1} $°C^{-1}$)	4185
Thermal conductivities of the mineral (W m^{-1} $°C^{-1}$)	2.5
Thermal conductivities of the water (W m^{-1} $°C^{-1}$)	0.6
Molecular diffusion (m^2 s^{-1})	1.5 10^{-10}
Mesh refinement (m)	0.025-20
Time step (month)	1
Division of the time step	33000

5. Numerical results and discussion

The numerical results for the single-layer model are predominantly focused on the mineralogical evolution whereas those for the multi-layer model mainly deal with porosity modifications and temperature profiles. According to the work of Castillo and co-workers [13], gibbsite, quartz, goethite, barite, anhydrite, hydromagnesite, and celestine were selected here as potential secondary minerals. Note that the hydromagnesite phase was considered instead of magnesite (another Mg-carbonate) because the latter forms at temperatures above 60–80 °C [43]. Similarly, precipitation of anhydrite rather than gypsum was assumed because the predicted temperatures were over 40 °C [44].

5.1. Single-layer geometry

Calcite alteration was observed in the near field of the injection well (from 0 to <1.5 m, Figure 5). The numerical results were affected by the modelling assumptions; calcite alteration decreased from “No degassing” to “Partial degassing” to “Total degassing” cases. Regardless of the injected fluids (Table 5), the model indicated dolomite dissolution up to about 15 m from the injection well occurring concomitantly to a calcite precipitation (from >1.5 to 15 m, Figure 5). Dolomite/ankerite conversion (approximately equivalent to dolomite/calcite conversion) has been observed in several experiments [45, 46]; thus, even if such reaction is probably overestimated (i.e. minerals processed at local equilibrium), a similar process is expected in the Dogger formation. Note that the amount of precipitated calcite was also promoted by the Ca concentrations in the injected fluids (Table 5) and the amount of mineral is lower for the “Total degassing” case. Regarding other mineralogical transformations, the amounts of microcline and albite remained constant. Considering the

low amounts of accessory minerals (illite and siderite) as well as precipitated secondary minerals (gibbsite, quartz, goethite, and barite), their impacts on porosity evolution were very limited; these numerical results are reported in the Supplementary Data. The formation of anhydrite, hydromagnesite, and celestine was not observed in any simulation case.

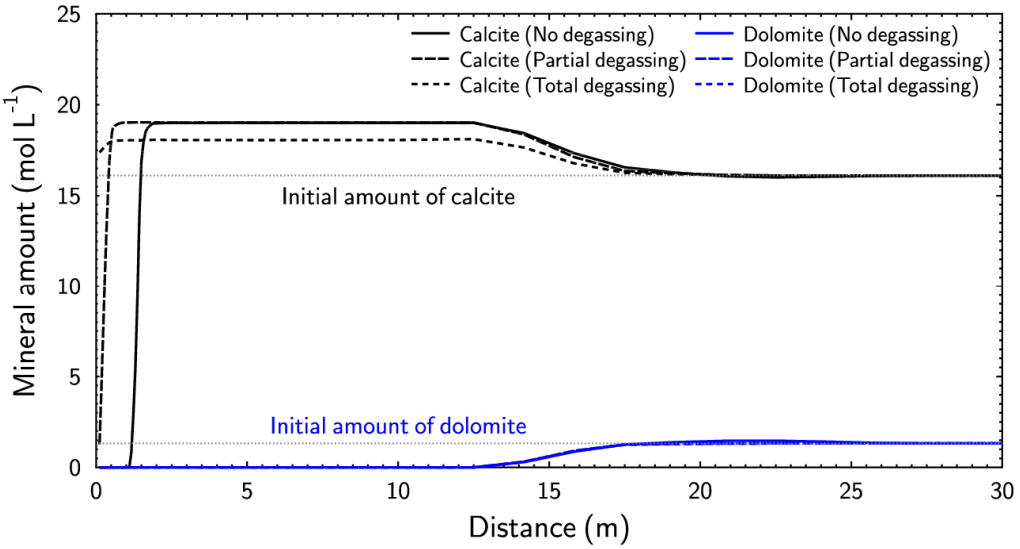

Figure 5. Calcite ($CaCO_3$) and dolomite ($CaMg(CO_3)_2$) profiles calculated with the single-layer model after 24 years of cooled brine injection. No degassing, partial degassing, and total degassing correspond to the different modelling cases based on injected fluid chemistry (see section 4.2).

As calcite and dolomite constitute 80% of the initial mineralogical assemblage of the Dogger formation (Table 2), modelling assumptions affected the resulting porosity (Figure 6a) while temperature profiles remained identical whatever the injected fluid chemistry (Figure 6b). The experimental results indicated an average radius of 0.21 m for the open hole. The modelling case omitting gas extraction ("No degassing" model) showed total dissolution of carbonate minerals up to 1 m around the injection well; the formation of an open hole around the injection well was clearly an overestimate. In contrast, the numerical modelling indicated that total degassing of the cooled injected fluid was unlikely as its effect on porosity was very limited (i.e. no significant variation around the injection well). Additionally, the low Ca concentration of the injected fluid (Table 5) limited the calcite precipitation promoted by the dolomite/calcite conversion and a slight porosity increase was predicted despite the molar volumes of minerals (i.e. 36.9 cm^3 mol^{-1} for $CaCO_3$ and 64.4 cm^3 mol^{-1} for $CaMg(CO_3)_2$). Finally, only partial CO_2 degassing of the injected fluid could explain the field observations.

According to the work of Deng and co-workers [47], dissolution of 35% is a reasonable threshold for a fast-reacting mineral (i.e. calcite), above which erosion of the altered layer occurs. Following the removal of the altered layer, the open-hole aperture increases. Assuming an initial porosity of 15% in the current model, a porosity increase of more than 50% would lead to disaggregation of the remaining matrix. The remaining minerals (e.g. albite and microcline) are expected to fall to the bottom of the injection well or be further transported. The “Partial degassing” model led to a porosity increase of up to 50% at 0.25 m (Figure 6a). An open-hole aperture of 0.25 m was then estimated, which is in reasonable agreement with the experimental data. Note that more recent doublets use two pumps to keep fluids under pressure and avoid the bubble point [48]. Therefore, the porosity profile obtained without degassing corresponds to the open-hole expected under such conditions.

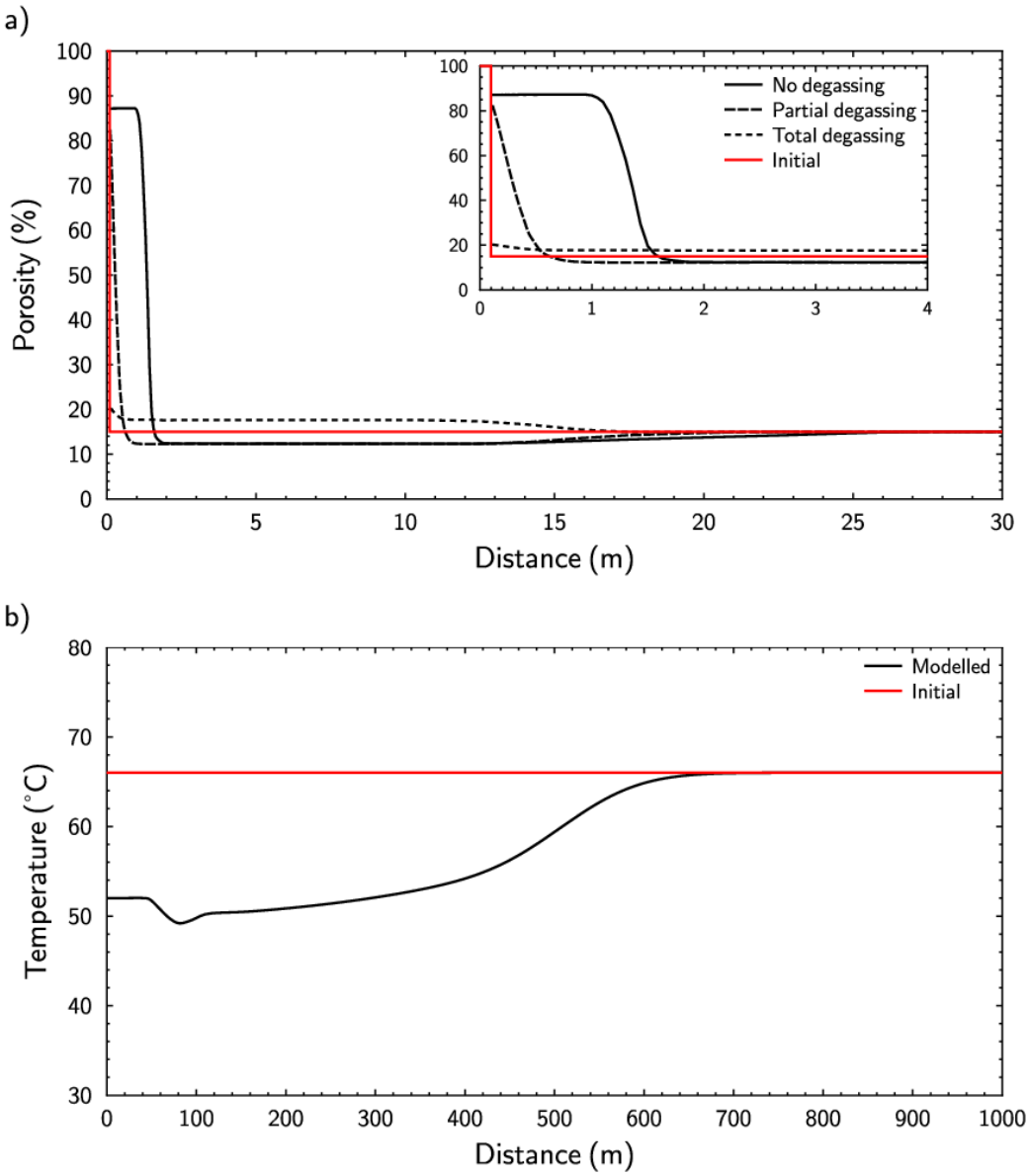

Figure 6. a) Porosity profile calculated with the single-layer model after 24 years of cooled brine injection. No degassing, partial degassing, and total degassing correspond to the different modelling cases based on injected fluid chemistry (see section 4.2). b) Temperature profile calculated with the single-layer model after 24 years of cooled brine; results are identical for all the injected fluid chemistries considered.

5.2. Multi-layer geometry

Mineralogical transformations calculated using the multi-layer model were similar to those already described with the single-layer model; the open-hole formation resulted in carbonate dissolution. Therefore, only the porosity profiles after 24 years of geothermal production are reported in Figure 7 whereas open-hole extensions are given in Table 7. As already observed with the previous model, the absence of fluid degassing led to an overestimation of open-hole formation (up to 6.2 m for layer 4). In contrast, the porosity change that was modelled assuming that total degassing was negligible. The best fit to the experimental data was obtained considering partial degassing of injected fluids. Assuming a threshold of 35% for carbonate alteration [47] and specific initial porosities for each layer (Table 1), the numerical results indicated an open-hole radius ranging from 0.37 m (layer 1) to 1.18 m (layer 4). Nonetheless, the reactivity of unproductive layers may buffer the alteration of productive layers, which is therefore likely to be overestimated if those unproductive layers are assumed to be impermeable. Such a reactivity is supported by experimental results effectively showing an alteration of layers identified as unproductive from flowmeter measurements (Figure 3). This explains why the use of a single-layer geometry allowed a better approximation of the alteration front progression in the Dogger aquifer.

Table 7. Open-hole extension modelled for the multi-layer geometry. No degassing, partial degassing and total degassing correspond to modelling assumptions made on fluid chemistries (see section 4.2)

Productive	Observed radius (m)		Modelled radius (m)		
layer	min-max	average	No degassing	Partial degassing	Total degassing
1	0.23-0.25	0.24 ±0.01	2.03	0.37	0.1*
2	0.21-0.28	0.24 ±0.02	2.96	0.56	0.1*
3	0.21-0.29	0.25 ±0.02	2.23	0.45	0.1*
4	0.14-0.25	0.19 ±0.05	6.16	1.18	0.1*
5	0.11-0.14	0.13 ±0.01	1.89	0.38	0.1*

* no extension, 0.1 m being the initial radius of the borehole

The geothermal doublet induces the formation of a “cold bubble” in the reservoir around the injector [1, 3]. The migration of the “cold bubble” was similar regardless of fluid chemistry assumptions and therefore, only one temperature profile is reported on Figure 8. After 24 years of geothermal production, the cold injection front progressed up to 700 m, which corresponds to half the distance between the injection and the production wells. The numerical results indicated that a decrease in temperature at the production well was unlikely and was in accordance with recorded data (i.e. no thermal breakthrough). Nonetheless, numerous studies have shown a dissymmetry of the temperature profile resulting from the shape of the velocity profile induced by fluid extraction at the production well [e.g. 13]; the production well has been neglected here as the modelling of the exact progression of the “cold bubble” was not an objective of this study. The consideration of two injection periods

(48 °C in winter and 52 °C in summer) led to an inhomogeneous temperature profile in the near field of the injection well. Consistent with the temperature dependence of the mineral solubility [30], both the temperature decrease and the mass transport led to a calcite alteration that was attenuated when enabling CO_2 degassing.

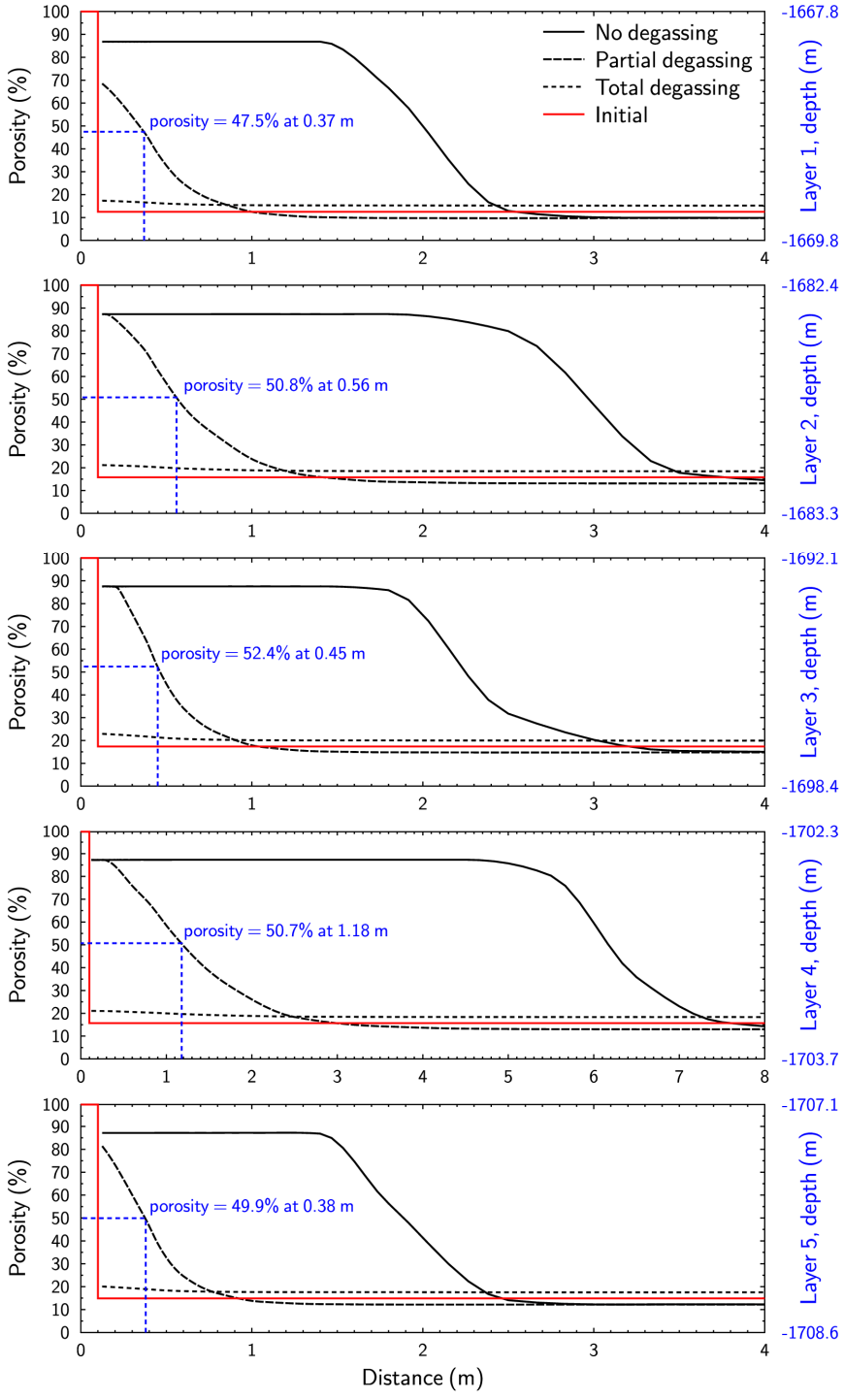

Figure 7. Porosity profile calculated with the multi-layer model after 24 years of cooled brine injection. No degassing, partial degassing and total degassing correspond to modelling assumptions made on fluid chemistries (see section 4.2).

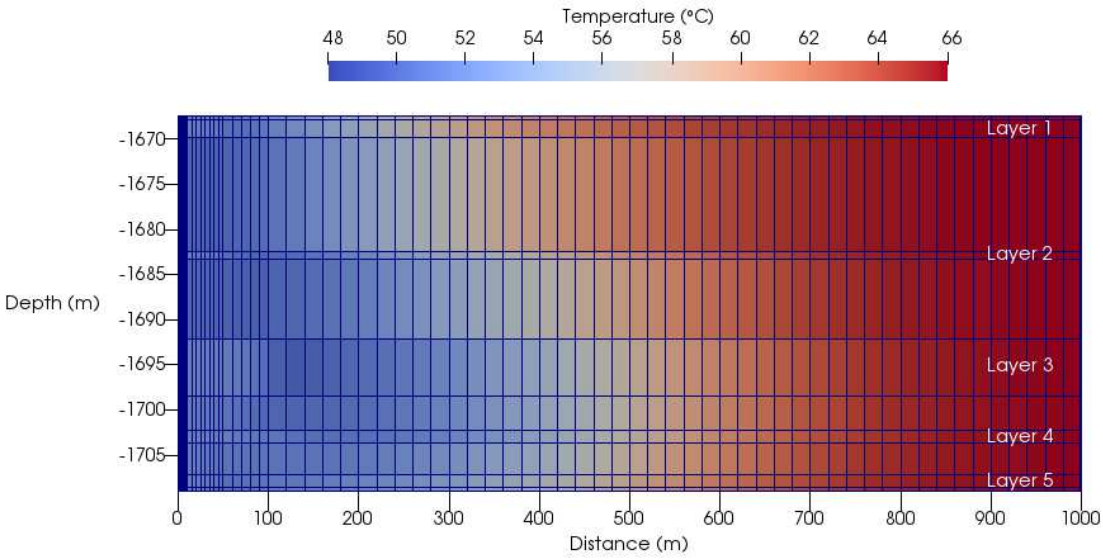

Figure 8. Temperature profile calculated with the multi-layer model after 24 years of cooled brine injection. Note that results were identical whatever modelling assumptions made on fluid chemistries (see section 4.2).

5.3. Model limitations

The modelling results of open-hole extension remain uncertain because several processes can affect its progression. The effects of porosity changes on the resulting permeability were neglected in this study. Following the Kozeny-Carman relationship, a porosity increase would lead to a permeability increase favouring mass transport and rock alteration. In contrast, the particles released by cement alteration could be mobilised and transported further, where particle re-deposition could cause clogging in the productive layer and a reduction of permeability [47, 49]. Unfortunately, the balance between higher porosity leading to higher permeability and porosity clogging by particles leading to a decrease of mass transport properties is difficult to determine. Therefore, our models assumed constant permeability and imposed average flow rates monitored at GCHE1. Moreover, the reinjection of cooled brine in the GCHE1 borehole could have a thermomechanical impact on the integrity of the reservoir rock that cannot be considered by MARTHE-PHREEQC. The current sonar technique is limited to the identification of open-hole walls and cannot detect porosity increases inside the rock matrix and/or the possible formation of wormholes in carbonated rock [18, 50]. However, despite these uncertainties, the model and field results were in

reasonable agreement, even if a simplified geometry was considered. Nevertheless, the non-iterative sequential coupling algorithm of the MARTHE-PHREEQC code implies using a relatively small time step fulfilling the Neumann criterion, thus leading to a high number of iterations and then a high computation time (i.e. several days). The time step used for this study (80 s, Table 7) is the best compromise between calculation efficiency and numerical dispersion possibly observed when the Neumann criterion is not strictly respected, which is the case for the smallest cells at the immediate vicinity of the well. However, keeping in mind that for all these cells, water-rock interactions rapidly became negligible as calcite was entirely dissolved, time step could be relaxed without negative consequence on calculation accuracy.

6. Conclusions

Field investigations of the Chelles former injection well after 24 years of continuous geothermal operation offered a novel opportunity to evaluate reservoir mineralogical transformations at the well outlet induced by cooled-brine reinjection during a typical geothermal exploitation period. Sonar data acquired on the open-hole part of this well showed significant and uneven distortion of the initial cylindrical geometry. The investigation technique, used for the first time in the Paris basin, is a promising tool for borehole examinations, especially when a camera is not practical due to groundwater turbidity as in the Dogger aquifer.

Using parameters as close as possible to actual well operation data as well as simplified geometries that are widely used in predictive modelling, this study attempted to quantify the water-rock interaction processes in the near-well area of the exploited reservoir. Because of the partial monitoring of production data and more specifically a lack of data on the chemistry of the injected fluids (e.g. rate of CO_2 degassing) as well as drawbacks of current reactive transport software (e.g. transport of eroded particles is not accounted for), the accuracy of the numerical results had some limitations. Nonetheless, the simulation results confirmed significant carbonate alterations in the near-well part of the reservoir on the same orders of magnitude as the average measured open-hole aperture (0.21 m). This gave us more confidence in our modelling approach and suggested that the observed geometry alteration could mainly have a geochemical origin. Best-fit results were obtained for partial CO_2 degassing in the reinjected brine, which is also consistent as the geothermal doublet was operated in artesian mode.

Although previous studies on the CO_2-DISSOLVED concept involving cooled CO_2-rich brine reinjection in a geothermal well (i.e. CO_2 concentration less than 1 mol L^{-1} under field

conditions, so that CO_2 remains entirely dissolved in brine) used a similar modelling approach, they lacked reference field data for evaluating the predictive capability of the models. Therefore, the results of this study, based on unique bottom-hole data showing the geochemical impact of brine reinjection in a "standard" geothermal doublet, constitute a valuable baseline for future calibration of reactive transport models. These reactive transport models could then be more confidently used to perform the pre-dimensioning calculations of dissolved CO_2 injection in a doublet, which forms the first operational test-phase of the CO_2-DISSOLVED system.

Acknowledgments

The authors thank the anonymous reviewers for their comments and suggestions. This work was supported by the ANR (French National Research Agency), within the framework of the "CO_2-DISSOLVED" project (ANR-12-SEED-0009), and Geodenergies (http://www.geodenergies.com/), as part of the "PILOTE CO_2-DISSOLVED" project. The authors would also like to thank Chelles Chaleur and Coriance for making the well available to our team during the three-day experimentation period. FLODIM are also greatly acknowledged for applying their proprietary sonar investigation tool to the novel context of a former geothermal injection well. The authors thank O. Audouin from CFG service for his technical support on the well characterisation.

References

[1] V. Hamm, M. Bouzit, S. Lopez, Assessment of complex well architecture performance for geothermal exploitation of the Paris basin: A modeling and economic analysis, Geothermics, 64 (2016) 300-313.

[2] S. Lopez, V. Hamm, M. Le Brun, L. Schaper, F. Boissier, C. Cotiche, E. Giuglaris, 40 years of Dogger aquifer management in Ile-de-France, Paris Basin, France, Geothermics, 39 (2010) 339-356.

[3] C. Castillo, M. Azaroual, I. Ignatiadis, O. Goyeneche, Geochemical Parameters as Precursors to Predict the Decline of Temperature in the Dogger aquifer (Paris Basin, France), in: Thirty-Sixth Workshop on Geothermal Reservoir Engineering, Stanford (California), United States, 2011, pp. 8p.

[4] E. Cordier, Modélisation numérique d'un doublet géothermique exploitant le Dogger dans le secteur de Bagneux dans le cadre de l'étude de faisabilité d'un doublet géothermal mise en œuvre par le SIPPEREC. Synthèse des calculs, in, 2013.

[5] C. Castillo, M. Azaroual, V. Hamm, N. Jacquemet, Physico-chimie et réactivité des fluides du Dogger du Bassin Parisien soumis aux conditions de stockage de chaleur, in, BRGM/RP-60189-FR, 2011.

[6] A.L. Gille, Suivi et modélisation du comportement hydro-géochimique du Dogger, soumis à la réinjection de fluides « chaud » et « froid », in, Université Pierre et Marie Curie, École nationale supérieure des Mines de Paris, Centre d'informatique Géologique de Fontainebleau., 2010.

[7] O. Borozdina, T. Ratouis, P. Ungemach, M. Antics, Thermochemical modelling of cooled brine injection into low enthalpy sedimentary reservoirs, Geothermal Resources Council Transactions, 36 (2012) 151-157.
[8] H.M. Nick, K.-H. Wolf, D. Brhun, Mixed CO2-Water Injection Into Geothermal Reservoirs: A Numerical Study, in: Proceedings World Geothermal Congress 2015 Melbourne, Australia, 2015.
[9] C. Wong, E. Buscarlet, S. Addison, M. Brun, Reactive Transport Modelling of Injection Fluid-Reservoir Rock Interaction, in: New Zealand Geothermal Workshop, Auckland, New Zealand, 2016.
[10] C. Kervévan, M.H. Beddelem, K. O'Neil, CO_2-DISSOLVED: a Novel Concept Coupling Geological Storage of Dissolved CO_2 and Geothermal Heat Recovery – Part 1: Assessment of the Integration of an Innovative Low-cost, Water- based CO_2 Capture Technology, Energy Procedia, 63 (2014) 4508-4518.
[11] C. Kervévan, F. Bugarel, X. Galiègue, Y. Le Gallo, F. May, K. O'Neil, J. Sterpenich, CO2-Dissolved: A novel approach to combining CCS and geothermal heat recovery, in: EAGE (Ed.) Sustainable Earth Sciences (SES), technologies for sustainable use of the deep sub-surface, Pau, France, 2013.
[12] C. Kervévan, M.H. Beddelem, X. Galiègue, Y. Le Gallo, F. May, K. O'Neil, J. Sterpenich, Main results of the CO2-DISSOLVED project: First step toward a future industrial pilot combining geological storage of dissolved CO2 and geothermal heat recovery, Energy Procedia, 114 (2017) 4086-4098.
[13] C. Castillo, N.C.M. Marty, V. Hamm, C. Kervévan, D. Thiéry, L. de Lary, J.-C. Manceau, Reactive Transport Modelling of Dissolved CO2 Injection in a Geothermal Doublet. Application to the CO2-DISSOLVED concept, Energy Procedia, 114 (2017) 4062-4074.
[14] F. Gray, B. Anabaraonye, S. Shah, E. Boek, J. Crawshaw, Chemical mechanisms of dissolution of calcite by HCl in porous media: Simulations and experiment, Advances in Water Resources, 121 (2018) 369-387.
[15] J. Snippe, S. Berg, K. Ganga, N. Brussee, R. Gdanski, Experimental and numerical investigation of wormholing during CO2 storage and water alternating gas injection, International Journal of Greenhouse Gas Control, 94 (2020) 102901.
[16] A. Randi, J. Sterpenich, C. Morlot, J. Pironon, C. Kervévan, M.H. Beddelem, C. Fléhoc, CO2-DISSOLVED: a Novel Concept Coupling Geological Storage of Dissolved CO_2 and Geothermal Heat Recovery – Part 3: Design of the MIRAGES-2 Experimental Device Dedicated to the Study of the Geochemical Water-Rock Interactions Triggered by CO_2 Laden Brine Injection, Energy Procedia, 63 (2014) 4536-4547.
[17] D. Thiéry, Modélisation 3D du Transport Réactif avec le code de calcul MARTHE v7.5 couplé aux modules géochimiques de PHREEQC, in: R. BRGM/RP-65010-FR (Ed.), Orléans, France, 2015, pp. 164, available at http://infoterre.brgm.fr/rapports/RP-65010-FR.pdf .
[18] A. Randi, J. Sterpenich, D. Thiéry, C. Kervévan, J. Pironon, C. Morlot, Experimental and numerical simulation of the injection of a CO2 saturated solution in a carbonate reservoir: Application to the CO2-DISSOLVED concept combining CO2 geological storage and geothermal heat recovery, Energy Procedia, 114 (2017) 2942-2956.
[19] O. Izgec, D. Zhu, A.D. Hill, Numerical and experimental investigation of acid wormholing during acidization of vuggy carbonate rocks, Journal of Petroleum Science and Engineering, 74 (2010) 51-66.
[20] M.M. Smith, Y. Sholokhova, Y. Hao, S.A. Carroll, CO2-induced dissolution of low permeability carbonates. Part I: Characterization and experiments, Advances in Water Resources, 62 (2013) 370-387.
[21] C. Massiot, D.D. McNamara, A. Nicol, J. Townend, Fracture width and spacing distributions from borehole televiewer logs and cores in the Rotokawa Geothermal Field, New Zealand, in: World Geothermal Congress 2015, International Geothermal Association, 2015.
[22] C. Massiot, J. Townend, A. Nicol, D.D. McNamara, Statistical methods of fracture characterization using acoustic borehole televiewer log interpretation, Journal of Geophysical Research: Solid Earth, 122 (2017) 6836-6852.
[23] L. De Lary, J.-C. Manceau, A. Loschetter, J. Rohmer, O. Bouc, I. Gravaud, C. Chiaberge, P. Willaume, T. Yalamas, Quantitative risk assessment in the early stages of a CO_2 geological storage

544 project: implementation of a practical approach in an uncertain context, Greenhouse Gases: Science
545 and Technology, 5 (2015) 50-63.
546 [24] C. Castillo, C. Kervévan, D. Thiéry, Geochemical and reactive transport modeling of the injection
547 of cooled Triassic brines into the Dogger aquifer (Paris basin, France), Geothermics, 53 (2015) 446-
548 463.
549 [25] P. Ungemach, Mise en service opérationnelle d'une ligne de dégazage : brûlage du biogaz
550 géothermal sur le doublet de Chelles, in: L'énergie du sous-sol. La géothermie en Ile-de-france.
551 Bulletin n°2, http://www.geothermie-perspectives.fr/sites/default/files/bulletin-gth-idf-02.pdf, 2001.
552 [26] B. Marty, A. Criaud, C. Fouillac, Low enthalpy geothermal fluids from the Paris sedimentary
553 basin—1. Characteristics and origin of gases, Geothermics, 17 (1988) 619-633.
554 [27] A. Criaud, C. Fouillac, B. Marty, M. Brach, H. F. Wei, Gas geochemistry of the Dogger geothermal
555 aquifer (Paris Basin, France), in: Twelfth Workshop on Geothermal Reservoir Engineering, Stanford
556 (California), United States, 1987.
557 [28] V. Hamm, J. Treil, M. Receveur, Gestion du Dogger et corrélation entre niveaux producteurs, in,
558 BRGM/RP-65472-FR, 2016.
559 [29] D.L. Parkhurst, C.A.J. Appelo, Description of input and examples for PHREEQC version 3 - A
560 computer program for speciation, batch-reaction, one-dimensional transport, and inverse
561 geochemical calculations, in, U.S. Geological Survey Techniques and Methods, , book 6, chap. A43,
562 497 p., available only at http://pubs.usgs.gov/tm/06/a43. , 2013.
563 [30] P. Blanc, A. Lassin, P. Piantone, M. Azaroual, N. Jacquemet, A. Fabbri, E.C. Gaucher,
564 Thermoddem: A geochemical database focused on low temperature water/rock interactions and
565 waste materials, Applied Geochemistry, 27 (2012) 2107-2116.
566 [31] T. Hörbrand, T. Baumann, H.C. Moog, Validation of hydrogeochemical databases for problems in
567 deep geothermal energy, Geothermal Energy, 6 (2018) 20.
568 [32] J. Trémosa, C. Castillo, C.Q. Vong, C. Kervévan, A. Lassin, P. Audigane, Long-term assessment of
569 geochemical reactivity of CO2 storage in highly saline aquifers: Application to Ketzin, In Salah and
570 Snøhvit storage sites, International Journal of Greenhouse Gas Control, 20 (2014) 2-26.
571 [33] L. André, P. Audigane, M. Azaroual, A. Menjoz, Numerical modeling of fluid–rock chemical
572 interactions at the supercritical CO2–liquid interface during CO2 injection into a carbonate reservoir,
573 the Dogger aquifer (Paris Basin, France), Energy Conversion and Management, 48 (2007) 1782-1797.
574 [34] J. Criaud, D. Giot, Y. Le Nindre, A. Criaud, C. Fouillac, M. Brach, A. Menjoz, J.-C. Martin, M.
575 Lambert, Caractérisation et modélisation du réservoir géothermique du Dogger, Bassin Parisien,
576 France., in, Rapport final BRGM-GTH, IRG SGN 89, 240 p., 1989.
577 [35] A. Coudrain-Ribstein, P. Gouze, G. de Marsily, Temperature-carbon dioxide partial pressure
578 trends in confined aquifers, Chemical Geology, 145 (1998) 73-89.
579 [36] E.C. Gaucher, C. Tournassat, F.J. Pearson, P. Blanc, C. Crouzet, C. Lerouge, S. Altmann, A robust
580 model for pore-water chemistry of clayrock, Geochimica et Cosmochimica Acta, 73 (2009) 6470-
581 6487.
582 [37] J.D. Rimstidt, H.L. Barnes, The kinetics of silica-water reactions, Geochimica et Cosmochimica
583 Acta, 44 (1980) 1683-1699.
584 [38] E. Bozau, S. Häußler, W. van Berk, Hydrogeochemical modelling of corrosion effects and barite
585 scaling in deep geothermal wells of the North German Basin using PHREEQC and PHAST,
586 Geothermics, 53 (2015) 540-547.
587 [39] G. Tarcan, Ü. Gemici, N. Aksoy, Hydrogeochemical factors effecting the scaling problem in
588 Balçova geothermal field, İzmir, Turkey, Environmental Geology, 58 (2008) 1375.
589 [40] T. Akin, A. Guney, H. Kargi, Modeling of Calcite Scaling and Estimation of Gas Breakout Depth in
590 a Geothermal Well by Using PHREEQC, in: Proceedings of the 40th Workshop on Geothermal
591 Reservoir Engineering, 2015.
592 [41] P. Vinsome, J. Westerveld, A simple method for predicting cap and base rock heat losses in
593 thermal reservoir simulators, Journal of Canadian Petroleum Technology, 19 (1980).
594 [42] M. Le Brun, V. Hamm, S. Lopez, P. Ungemach, M. Antics, J. Yves Ausseur, E. Cordier, E. Giuglaris,
595 P. Goblet, P. Lalos, Hydraulic and thermal impact modelling at the scale of the geothermal heating

596 doublet in the Paris Basin, France, in: 36th Stanford Geothermal Workshop, Stanford, United States,
597 2011, pp. 403-416.
598 [43] Q. Gautier, P. Bénézeth, V. Mavromatis, J. Schott, Hydromagnesite solubility product and growth
599 kinetics in aqueous solution from 25 to 75 °C, Geochimica et Cosmochimica Acta, 138 (2014) 1-20.
600 [44] A.E. Hill, The Transition Temperature of Gypsum to Anhydrite, Journal of the American Chemical
601 Society, 59 (1937) 2242-2244.
602 [45] M. Debure, P. Andreazza, A. Canizarès, S. Grangeon, C. Lerouge, P. Mack, B. Madé, P. Simon, E.
603 Veron, F. Warmont, M. Vayer, Study of Iron-Bearing Dolomite Dissolution at Various Temperatures:
604 Evidence for the Formation of Secondary Nanocrystalline Iron-Rich Phases on the Dolomite Surface,
605 ACS Earth and Space Chemistry, 1 (2017) 442-454.
606 [46] A.P. Gysi, A. Stefánsson, CO2-water–basalt interaction. Low temperature experiments and
607 implications for CO2 sequestration into basalts, Geochimica et Cosmochimica Acta, 81 (2012) 129-
608 152.
609 [47] H. Deng, M. Voltolini, S. Molins, C. Steefel, D. DePaolo, J. Ajo-Franklin, L. Yang, Alteration and
610 Erosion of Rock Matrix Bordering a Carbonate-Rich Shale Fracture, Environmental Science &
611 Technology, 51 (2017) 8861-8868.
612 [48] D. Lenoir, Geothermal exploitation of the Dogger in the Paris basin maintenance, renewal and
613 reliability of the geothermal loop, Geothermics, 21 (1992) 855-860.
614 [49] M.A. Sbai, M. Azaroual, Numerical modeling of formation damage by two-phase particulate
615 transport processes during CO2 injection in deep heterogeneous porous media, Advances in Water
616 Resources, 34 (2011) 62-82.
617 [50] H. Ott, S. Oedai, Wormhole formation and compact dissolution in single- and two-phase CO2-
618 brine injections, Geophysical Research Letters, 42 (2015) 2270-2276.

619

620